

# Formation Maneuvers in Three Dimensions\*

Hall, James K.<sup>1</sup>, and Meir Pachter<sup>2,3</sup>  
Air Force Institute of Technology  
Wright-Patterson Air Force Base, OH 45433

## ABSTRACT

The flying of aircraft in formation necessitates the extension of the theory of formation flight control to allow for three dimensional formation maneuvers. A leader and wingman formation is considered. A rotating reference frame attached to the wingman is used and special attention is given to the motion of the leader relative to the wingman. A seven state, three input, and three disturbance signal control system which models the dynamics of a two-aircraft formation in three dimensional space is developed. Two formation flight control concepts are investigated. A proportional, integral, and derivative automatic control system to maintain the wing aircraft in the specified formation geometry despite the leader's maneuvers is designed, and its performance is examined in simulation experiments.

## 1. INTRODUCTION

It has recently been shown that close formation flying of aircraft affords a significant reduction in induced drag, thereby extending the range of the entire formation, [1]. In this paper, a two-aircraft, leader and wingman, formation is considered. The principal challenge to applying the close formation flight concept is the requirement for constant pilot attention to maintain the tight positional tolerances needed in order to realize the maximum drag reduction benefit. Relieving pilot workload associated with such precise formation flying motivates our research into automating the wingman's control task. Thus, an automatic formation controller for the wing aircraft is desired, one that will maintain a specified formation geometry despite the three dimensional maneuvers flown by the leader. In [2] and [3], the formation dynamics are confined to the horizontal plane. The objective of this paper is to further the development of automatic formation flight control systems by extending previous work documented in [2], [3] and the references therein, and in [4], to include full three dimensional formation dynamics.

In this paper, the subscript W refers to the aircraft flying in the wingman position in the formation and the subscript L refers to the aircraft leading the formation. Each aircraft is considered to be a point mass, and a model is established of the formation's three dimensional dynamics. A rotating reference frame attached to the wingman is used and special attention is given to the motion of the leader relative to the wingman. A seven state, three input, and three disturbance signal control system which models the dynamics of a two-aircraft formation in three dimensional space is developed. In [1], it is shown that to achieve the maximal reduction in induced drag from flying in formation, there is an optimal separation geometry that must be maintained to tight tolerances: W is to be placed in the same x-y plane as L, with a longitudinal separation distance of three times L's wing span and a lateral separation distance of approximately  $\pi/4$  times L's wing span. A proportional, integral, and derivative (PID) automatic control system for the wing aircraft that maintains the specified formation despite the leader's maneuvers is designed, and its performance is examined.

In section 2, the rotating frame of reference attached to W's instantaneous position and aligned with W's wind axes is introduced. The three dimensional formation dynamics are developed in Section 3. Two candidate PID formation flight controllers are discussed in Section 4. The controllers' performance is discussed with reference to different formation types by way of simulation results, presented in Section 5, followed by conclusions in Section 6.

## 2. FRAME OF REFERENCE

Formation flight control necessitates the use of rotating frames of reference. The equations of motion are derived using a translating and rotating frame of reference collocated with the instantaneous position of W. The rotating frame of reference, shown in Fig. 1, is a triad of wind axes defined as follows: the x-axis is aligned with the aircraft velocity vector, the z-axis is aligned with the lift vector, and the y-axis (out the left wing) completes the right-handed coordinate system. The wind axes frame's attitude is specified by the  $\psi$ ,  $\gamma$ , and  $\phi$  Euler angles. For the sake of clarity, the final rotation about the  $x_w$  axis through the angle  $\phi$  is not explicitly shown in Fig. 1. Since a point mass model is used, moments are not included in

1. Captain, US Air Force

2. Professor, Dept. of Electrical and Computer Engineering

3. Corresponding Author e-mail mpachter@afit.af.mil

\*The views expressed in this article are those of the authors and do not reflect the official policy or position of the United States Air Force, Department of Defense, or U.S. Government.

the analysis. In the absence of the L vortex filaments [3] and [4], the derivation assumes no aerodynamic side force, viz. no sideslip. However, the possibility of an aerodynamic side force,  $Y_W$ , induced by L's vortex filaments, is allowed for and is included in the derivation.

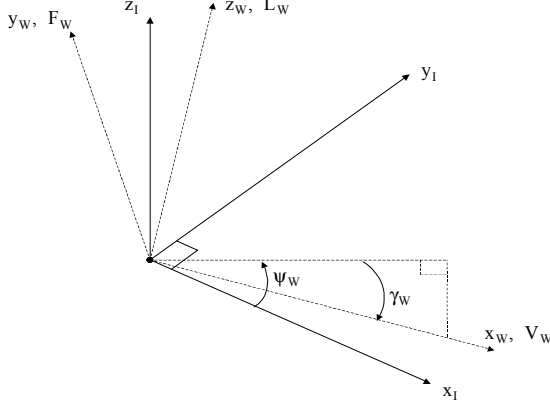


Figure 1. Inertial and W Axes.

### 3. EQUATIONS OF MOTION

Formation equations of motion for the rate of change of the three state variables of W are derived from Newton's Laws. A key aspect of the three dimensional derivation is the instantaneous angular rate,  $\bar{\omega}_W$ , of W's wind axes triad, which is attached to W's three dimensional trajectory. Also fundamental to the problem of formation flight is the relative position of the two aircraft. Therefore, the position and attitude of the wind axes systems for both W and L need to be related to an inertial reference frame, denoted with the subscript I, as depicted in Fig. 2.

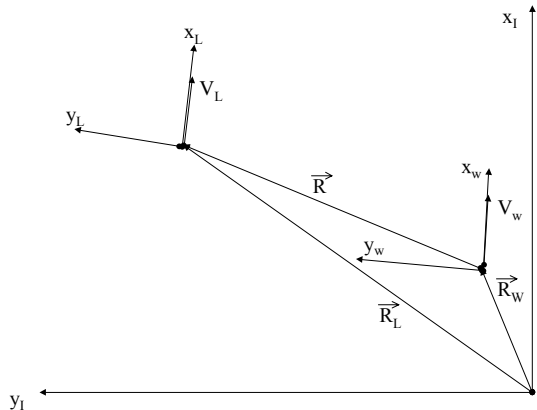


Figure 2. Three reference frames (view from above).

The vectors  $\bar{r}_L$  and  $\bar{r}_W$  in Fig. 2 are resolved in the inertial reference frame and the vector  $\bar{r}$  is resolved in the rotating frame attached to W. The change in position of L with respect to time can be written as the summation of the

change in W's position and the change in separation distance,  $\bar{r}$ , to which the Coriolis equation is then applied. Thus,

$$\frac{D\bar{r}}{Dt} = \frac{D\bar{r}_W}{Dt} + \frac{d\bar{r}}{dt} + \bar{\omega}_W \times \bar{r} \quad (1)$$

where the reference frame's angular rate is

$$\bar{\omega}_W = \begin{bmatrix} P_W \\ Q_W \\ R_W \end{bmatrix}$$

The angular rates shown above can be related to the Euler angles by using the following relationship, adapted from [5]:

$$\begin{bmatrix} P \\ Q \\ R \end{bmatrix} = \begin{bmatrix} 1 & 0 & -\sin \gamma \\ 0 & \cos \phi & \sin \phi \cos \gamma \\ 0 & -\sin \phi & \cos \phi \cos \gamma \end{bmatrix} \begin{bmatrix} \dot{\phi} \\ \dot{\gamma} \\ \dot{\psi} \end{bmatrix}$$

Using this relationship and the time rate of change of the  $\gamma$  and  $\psi$  Euler angles found from Newton's laws; see, e.g., Eqs. (5) and (7) in this section; the angular rates can be expressed according to the following three equations:

$$P_W = \dot{\phi}_W + \frac{\tan \gamma_W (L_W \sin \phi_W - Y_W \cos \phi_W)}{m_W V_W} \quad (2a)$$

$$Q_W = -\frac{L_W}{m_W V_W} + \frac{g \cos \gamma_W \cos \phi_W}{V_W} \quad (2b)$$

$$R_W = -\frac{g \cos \gamma_W \sin \phi_W}{V_W} + \frac{Y_W}{m_W V_W} \quad (2c)$$

Direction cosine matrices  $C_W$  and  $C_L$  transform from the rotating to the inertial axes systems, and are formed by multiplying, in order, the three single-axis-of-rotation matrices. The generic C matrix shown below is applicable to both L and W according to whether L's or W's Euler angles are used.

$$C = \begin{bmatrix} \cos \psi \cos \gamma & \cos \psi \sin \gamma \sin \phi - \sin \psi \cos \phi & \sin \psi \sin \phi + \cos \psi \sin \gamma \cos \phi \\ \sin \psi \cos \gamma & \cos \psi \cos \phi + \sin \psi \sin \gamma \sin \phi & -\cos \psi \sin \phi + \sin \psi \sin \gamma \cos \phi \\ -\sin \gamma & \cos \gamma \sin \phi & \cos \gamma \cos \phi \end{bmatrix}$$

Using this matrix and Eq. (1), the velocity relationship can be transformed into the inertial reference frame and the rate of change in separation distance, measured in the W rotating reference frame, can be written as

$$\begin{bmatrix} \dot{x} \\ \dot{y} \\ \dot{z} \end{bmatrix} = \frac{d\bar{r}}{dt} = \begin{bmatrix} R_W y - Q_W z \\ P_W z - R_W x \\ Q_W x - P_W y \end{bmatrix} + V_L C_W^T \begin{bmatrix} \cos \gamma_L \cos \psi_L \\ \cos \gamma_L \sin \psi_L \\ -\sin \gamma_L \end{bmatrix} - V_W \begin{bmatrix} 1 \\ 0 \\ 0 \end{bmatrix} \quad (3)$$

The final step in the derivation is to insert the angular rates from Eqs. (2a) – (2c) into Eq. (3).

The pertinent equations of motion for a two-aircraft formation relate the velocities and attitudes of the aircraft and the distance separating them. Thus, the state variables of the two-aircraft formation flight control system are:  $V_W$ ,  $\gamma_W$ ,  $\psi_W$ ,  $\phi_W$ ,  $x$ ,  $y$ ,  $z$ ,  $V_L$ ,  $\gamma_L$ , and  $\psi_L$  ( $\in \mathfrak{R}^{10}$ ). However, by introducing the heading error state,  $\psi_e$ ,

as the difference between the L and W heading angles,  $\psi_L$  and  $\psi_W$ , respectively, the order of the model can be reduced by one. Consistent with the formation flight control problem statement, an additional simplification can be made by declaring L's states exogenous disturbances. Thus, the original ten formation states are reduced to the following seven states:  $V_W$ ,  $\gamma_W$ ,  $\phi_W$ ,  $\psi_e$ ,  $x$ ,  $y$ , and  $z$  ( $\in \mathfrak{R}^7$ ). The three control variables for the system are:  $L_W$ ,  $T_W$ , and  $p_W$  ( $\in \mathfrak{R}^3$ ), where  $p_W$  is defined as the time rate of change of W's bank angle,  $\dot{\phi}_W$ . The exogenous disturbances are the velocity, heading angle, and the y component of lift of the lead aircraft:  $V_L$ ,  $\gamma_L$ , and  $L_L \sin \phi_L$ . Additional exogenous variables are the commanded formation geometry separation distances:  $x_c$ ,  $y_c$  and  $z_c$ . Thus, the seven differential equations of motion that model the two-aircraft system are as follows:

$$\dot{V}_W = \frac{T_W - D_W}{m_W} + g \sin \gamma_W \quad (4)$$

$$\dot{\gamma}_W = \frac{-L_W \cos \phi_W - Y_W \sin \phi_W}{m_W V_W} + \frac{g \cos \gamma_W}{V_W} \quad (5)$$

$$\dot{\phi}_W = p_W \quad (6)$$

$$\dot{\psi}_e = -\frac{L_L \sin \phi_L}{m_L V_L \cos \gamma_L} + \frac{L_W \sin \phi_W - Y_W \cos \phi_W}{m_W V_W \cos \gamma_W} \quad (7)$$

$$\dot{x} = \frac{-y g \cos \gamma_W \sin \phi_W - z g \cos \gamma_W \cos \phi_W}{V_W} + \frac{y Y_W + z L_W}{m_W V_W} - V_W + V_L (\cos \gamma_W \cos \gamma_L \cos \psi_e + \sin \gamma_W \sin \gamma_L) \quad (8)$$

$$\dot{y} = z p_W + \frac{z \tan \gamma_W (L_W \sin \phi_W - Y_W \cos \phi_W) - x Y_W}{m_W V_W} + \frac{x g \cos \gamma_W \sin \phi_W}{V_W} + V_L (\sin \gamma_W \cos \gamma_L \sin \phi_W \cos \psi_e + \cos \gamma_L \cos \phi_W \sin \psi_e - \cos \gamma_W \sin \gamma_L \sin \phi_W) \quad (9)$$

$$\dot{z} = -y p_W + \frac{-y \tan \gamma_W (L_W \sin \phi_W - Y_W \cos \phi_W) - x L_W}{m_W V_W} + \frac{x g \cos \gamma_W \cos \phi_W}{V_W} + V_L (\sin \gamma_W \cos \gamma_L \cos \phi_W \cos \psi_e - \cos \gamma_L \sin \phi_W \sin \psi_e - \cos \gamma_W \sin \gamma_L \cos \phi_W) \quad (10)$$

The point mass modeling of W using the wind axes coordinate system definition is the basis for the derivation of Eqs. (4) – (7), and Eqs. (8) – (10) are derived from Eqs. (2) and (3). The drag,  $D_W$ , can be eliminated from the velocity equation by solving for drag as a function of lift. Thus, Eq. (4) can be rewritten assuming a

parabolic drag polar specified with the constants  $C_{D0W}$  and  $K_W$ ,

$$\dot{V}_W = \frac{T_W - \bar{q}_W S_W C_{D0W} - \frac{K_W L_W^2}{\bar{q}_W S_W}}{m_W} + g \sin \gamma_W \quad (11)$$

Eqs. (5) – (11) are the nonlinear model of the two-aircraft formation dynamics used in the controller design and in the simulations.  $Y_W$  denotes an aerodynamic side force, which is set equal to zero in this paper.

#### 4. FORMATION FLIGHT CONTROLLER

A PID formation flight controller is designed. The three control channels,  $x$ ,  $y$ , and  $z$ , employ PID control action. Thrust control is affected in the  $x$  channel, which is to say that any difference in the commanded and the actual value of  $x$  separation between the two aircraft, results in a change in thrust. Similarly, lift is the control variable in the  $z$  channel and roll rate is the control variable in the  $y$  channel. Eqs. (12) – (14) specify the PID control law for each of the three control variables:  $T_W$ ,  $L_W$ , and  $p_W$ , respectively.

$$T_W = K_{T_P} e_x + K_{T_D} \dot{e}_x + K_{T_I} \int e_x dt \quad (12)$$

$$L_W = K_{L_P} e_z + K_{L_D} \dot{e}_z + K_{L_I} \int e_z dt \quad (13)$$

$$p_W = K_{p_P} e_y + K_{\psi} \psi_e + K_{p_D} \dot{e}_y + K_{p_{DD}} \ddot{e}_y + K_{p_I} \int e_y dt \quad (14)$$

where the error signals are

$$\begin{bmatrix} e_x \\ e_y \\ e_z \end{bmatrix} = \begin{bmatrix} x_c - x \\ y_c - y \\ z_c - z \end{bmatrix} \quad (15)$$

The integral of each error signal is created by augmenting the formation equations of motion. The derivative control elements are created by differencing the separation distances for each time step and dividing by the magnitude of the time step. Control in the lateral channel required the use of a second difference term for roll rate and proportional feedback of the heading error.

Note that by a dynamic inversion argument, the roll rate command,  $P_W$ , is obtained according to Eqs. (14) and (2a), viz.,

$$P_W = K_{p_P} e_y + K_{\psi} \psi_e + K_{p_D} \dot{e}_y + K_{p_{DD}} \ddot{e}_y + K_{p_I} \int e_y dt + \frac{\tan \gamma_W (L_W \sin \phi_W - Y_W \cos \phi_W)}{m_W V_W} \quad (16)$$

Also note that for a formation, right turns and left turns have dissimilar dynamics, dependent upon W's position in the  $y$  direction. This is similar to running on a track, where the runner on the inside lane has to turn sharper (on a shorter path) to stay in his lane.

In an attempt to more closely mimic actual pilot control inputs, an alternative control law is also devised. For this new control law, the need for W to climb, according to a separation error in the z direction, results in the controller responding with increased thrust, whereas the need for W to increase flight speed causes the lift to decrease. In other words, thrust is now the control variable in the z channel and lift is the control variable in the x channel. As before, roll rate is the control variable in the y channel. The alternate control law is

$$T_W = K_{T_P} e_z + K_{T_D} \dot{e}_z + K_{T_{DD}} \ddot{e}_z + K_{T_I} \int e_z dt \quad (17)$$

$$L_W = K_{L_P} e_x + K_{L_D} \dot{e}_x + K_{L_{DD}} \ddot{e}_x + K_{L_I} \int e_x dt \quad (18)$$

For this paper, Eqs. (12) – (14) will be referred to as the first control law and Eqs. (14), (17) and (18) will be referred to as the second control law.

Furthermore, pilots fly two different formations during turns. In the first type of formation turn, L remains in W's x-y plane. This is the method used for the design of the formation flight control system in this paper, and can be thought of as a pseudo-wingtip formation, dependent on how closely the controller is able to match the attitude and translation of L. In a route formation, W and L remain in the same inertial x-y plane during the turn. To implement this controller, the error signals in Eq. (15) must be transformed into the inertial frame of reference, according to the matrix operation shown below,

$$\begin{bmatrix} e_x \\ e_y \\ e_z \end{bmatrix} = C_W \begin{bmatrix} x_c - x \\ y_c - y \\ z_c - z \end{bmatrix},$$

prior to the application of the PID control laws. In a true wingtip formation, the controller maintains W in L's x-y plane throughout the turn. This type of formation controller is implemented by transforming the error signals in Eq. (15) into the L reference frame according to

$$\begin{bmatrix} e_x \\ e_y \\ e_z \end{bmatrix} = -C_L^T C_W \begin{bmatrix} x_c - x \\ y_c - y \\ z_c - z \end{bmatrix},$$

prior to the application of the PID control laws.

## 5. SIMULATION RESULTS

The formation flight control system's response to the leader's maneuvers and commanded changes in formation geometry ( $x_c$ ,  $y_c$  and  $z_c$ ) was simulated using the full, nonlinear equations of motion for the two-aircraft system, given in Eqs. (5) – (11). The airplanes modeled in the simulation are both F-16 class aircraft. The simulation has the formation initially flying at an altitude of 15,000 meters and at an airspeed of 0.85 Mach, or approximately 251.5 meters per second. Table 1 shows the values of the

drag polar constants ( $C_{D_0}$  and K) that were used to determine the thrust required for trimmed flight. Naturally, the lift is equal to the weight during trimmed flight. For this size of aircraft the optimal formation geometry for induced drag reduction, as measured in the W reference frame, was  $x_c = 27$  meters,  $z_c = 0$  meters, and  $y_c = 7$  meters in the positive or negative y direction.

Table 1. Aircraft Specifications

|                               |           |                         |
|-------------------------------|-----------|-------------------------|
| Wing Area                     | S         | 27.87 [m <sup>2</sup> ] |
| Wing Span                     | b         | 9.14 [m]                |
| Aspect Ratio                  | AR        | 3                       |
| Coefficient of Zero-Lift Drag | $C_{D_0}$ | 0.015                   |
| Drag Polar Constant           | K         | 0.02                    |
| Mass                          | m         | 11336.4 [kg]            |

Initially, the formation flight control system was exercised by commanding W to perform a one meter repositioning in each of the three Cartesian axes directions. The control system gains were selected to ensure the aircraft would properly reach the correct formation position. Fig. 3 shows the controller's performance, by way of time histories, in response to the one meter step commands.

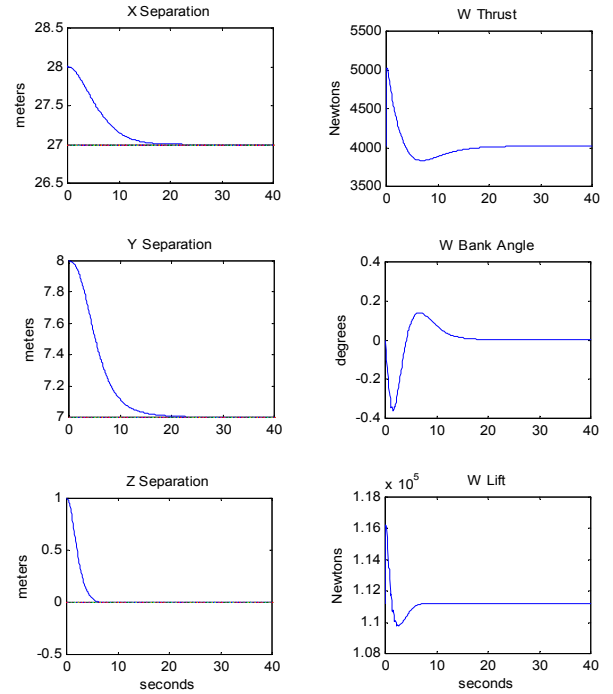


Figure 3. Formation geometry change.

Next, L is flown through three different maneuvers and it is shown that the formation is maintained. The three maneuvers investigated are: L accelerating to a new velocity, L changing altitude, and L changing heading. Note that the no sideslip requirement mandates that all heading changes be accomplished by rolling the aircraft. Thus, the W controller is required to perform full three dimensional maneuvers, or in other words, the heading change is a kinematically coupled

maneuver, where all three control channels are exercised and adjustments to any control channel affects the other channels.

Fig. 4 shows how W responds when L's velocity is increased by 10 meters per second. The velocity lag in W is minimal, and the thrust increases according to the x separation distance, and settles at a new steady state value that is somewhat greater than at the initial trim condition, as expected. Thus, automatic retrimming, which is provided by integral action, is achieved.

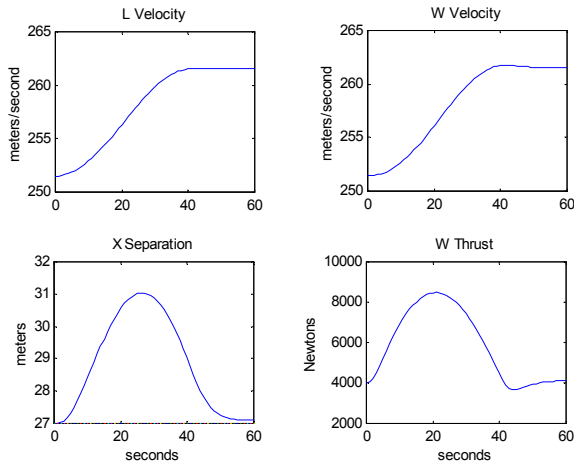


Figure 4. W's response to L velocity increase.

The second pitch plane maneuver entailed an L altitude increase. Note, in Fig. 5, that the pitch angle of W goes from zero degrees to negative five degrees and back to zero in climbing to the new altitude. This is consistent with the definition of positive pitch in the wind axes system as shown in Fig. 1. The excursion in x separation shown in Fig. 5 becomes fairly large due to L being flown at a constant velocity and W temporarily losing speed as it pitches up. L's changing pitch angle is reflected in the changing z separation.

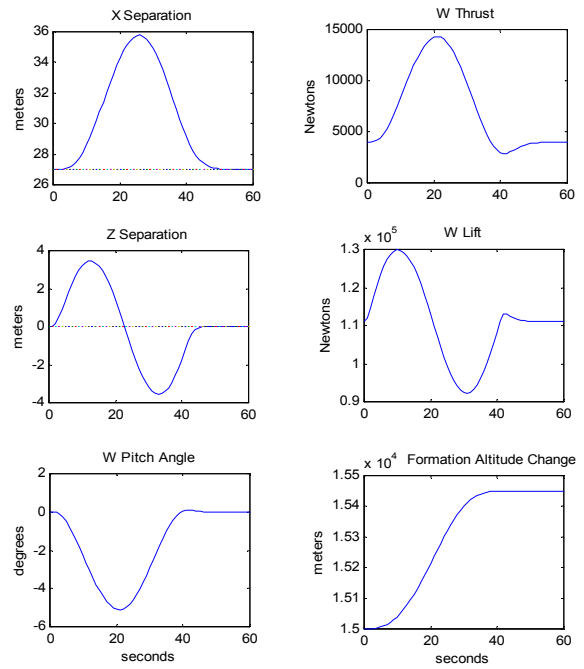


Figure 5. W's response to L altitude increase.

The third L maneuver is a heading change. Because of the definition of the wind axes system, a positive heading change is produced by rolling to the left. In this maneuver, W was positioned to the right of L and therefore followed the outside track. It is important to realize that the separation distances in the simulation are measured in the W rotating reference frame. This results in separation distances that are a function of W's orientation, as well as the inertial spacing of the aircraft centers of gravity. Fig. 6 shows the roll angle and lift of L as it performs the heading change maneuver.

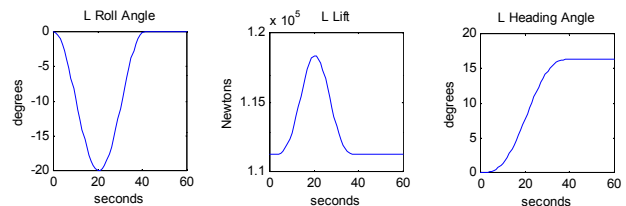


Figure 6. L heading change maneuver.

The separation distances measured in the inertial reference frame have been included to provide further insight into the dynamics of the maneuver. Fig. 7 shows the increase in thrust required to maintain level flight, and the increase in velocity needed to maintain formation while W flies a larger radius turn.

The next series of Figures show the first and second control systems responding to the exogenous disturbance created by L flying the maneuver shown in Fig. 6. Again, W's position and attitude relative to L is the main concern. The Figures show all three control channels compensating simultaneously, evidence of the complex nature of flying lateral maneuvers. The separation

distances measured in the inertial reference frame are also shown to illustrate the differences between measurements in the two reference frames during this maneuver.

The control system attempted to position W so that L was in W's x-y plane. This is approximately a wingtip formation turn if W rotates through the same bank angle as L and the z separation distance, measured in W's reference frame is very small. Also included is the z channel response when a route formation turn is commanded.

The velocity increase in Fig. 7 is due to the larger turn radius flown by W. In order to maintain the formation, W has to travel at a greater velocity. Note the difference in the final value of the inertial separation distance compared to the W reference frame separation distance.

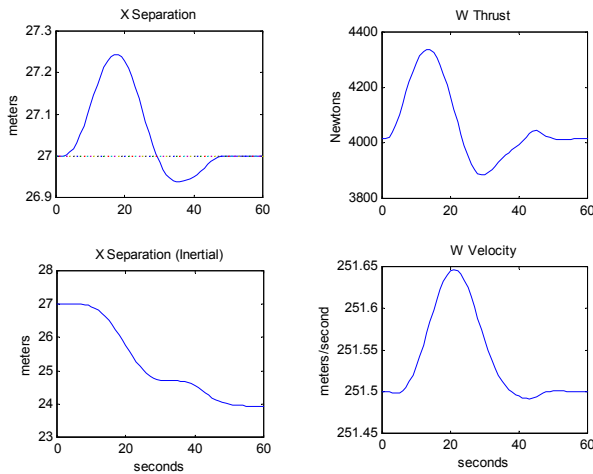


Figure 7. W's response to L heading change: x axis.

Comparing the x channel response of the first control system, shown above, with the second, shown in Fig. 8, the x separation actually decreases during the turn, which is consistent with the corresponding increase in velocity. The lift commanded by the first controller, see Fig. 11, is only slightly less than that commanded by the second controller.

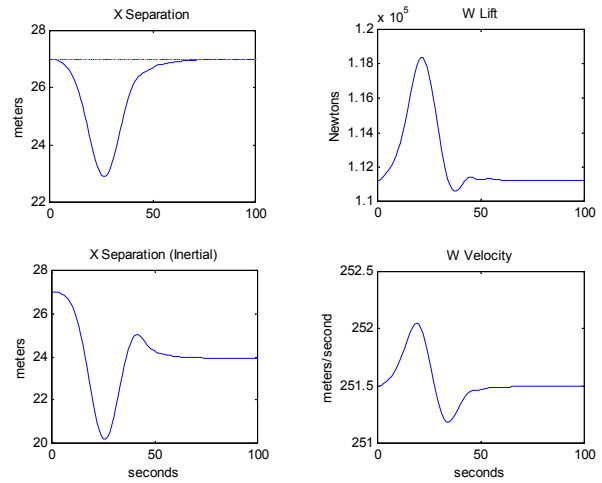


Figure 8. W's response to L heading change: second control law: x axis.

The y separation distances shown in Fig. 9 result from L banking to the left and flying away from W initially and then rolling back to level flight. Comparing the roll angle of W (Fig. 9) with that of L (Fig. 6), the time histories are nearly identical, with only a slight overshoot by the control system, as expected. Because the roll angles match so closely, this maneuver is a good approximation for a wingtip formation turn. Again, the Cartesian components of the separation distance are dramatically different in the rotating and inertial frames. Naturally, the magnitude of the scalar formation separation distance is the same in both reference frames.

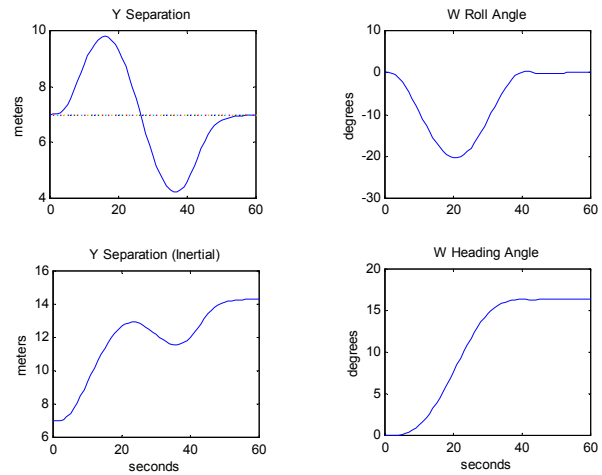


Figure 9. W's response to L heading change: y axis.

The exercise of the second control law has very little effect on the y channel response, except that the system response is somewhat slower and the separation distance transients, shown in Fig. 10, are greater than for the first control system. Although the transient response is different, the formation is maintained and both separation distances have the same steady state value as for the first controller in Fig. 9.

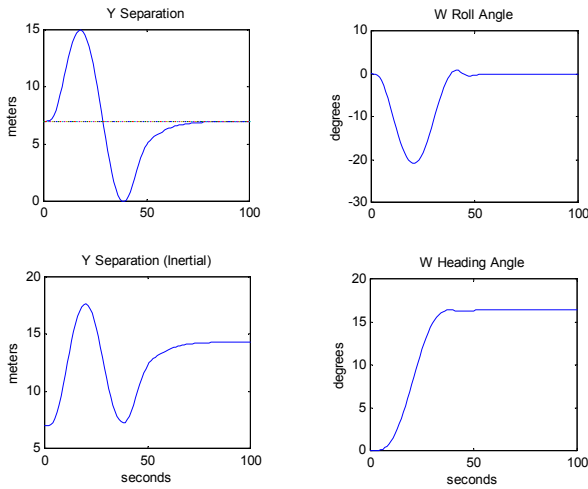


Figure 10. W's response to L heading change: second control law: y axis.

The z channel controller, shown in Fig. 11, responded with a dramatic increase in lift, as would be expected to maintain altitude during a coordinated turn. Note the large difference in the transients of the z separation distance measured in the two reference frames. The inertial frame shows a larger value of z separation excursion, indicating the strong effect of roll angle on measured distance. The comparatively small value of separation distance in the W frame is the result of the formation turn type flown by the control system, i.e., the controller is trying to keep L in W's x-y plane, giving a good approximation of a wingtip formation turn. As mentioned earlier, this is accomplished by feeding back the separation distance errors measured in W's reference frame.

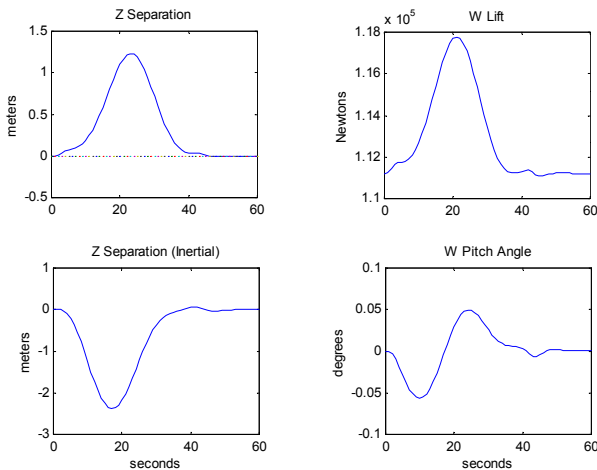


Figure 11. W's response to L heading change: z axis.

To compare commanded thrust of the two control laws, refer to Fig. 7 for the first and Fig. 12 for the second; the second control system requires larger thrust variations to maintain the formation. This is consistent with what was seen in the x channel and y channel responses shown

previously. Also, the separation distance transients are larger for the second controller than for the first controller.

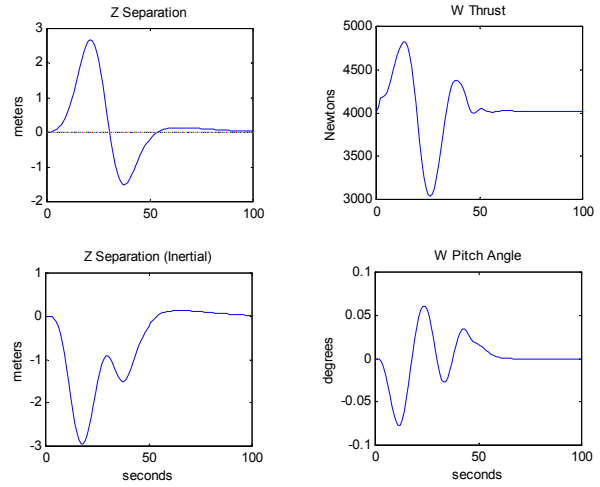


Figure 12. W's response to L heading change: second control law: z axis.

Optional formation strategies are available when conducting turning maneuvers. The principal approach in the simulations was to have the W control system maintain L in W's x-y plane, which is to say, a z separation distance equal to zero is enforced to approximate a wingtip formation turn. Fig. 13 shows an approximate route formation turn, where the W control system is working to fly L and W in the same inertial x-y plane. Notice that the separation distance transients in the inertial reference frame are smaller than in the W reference frame.

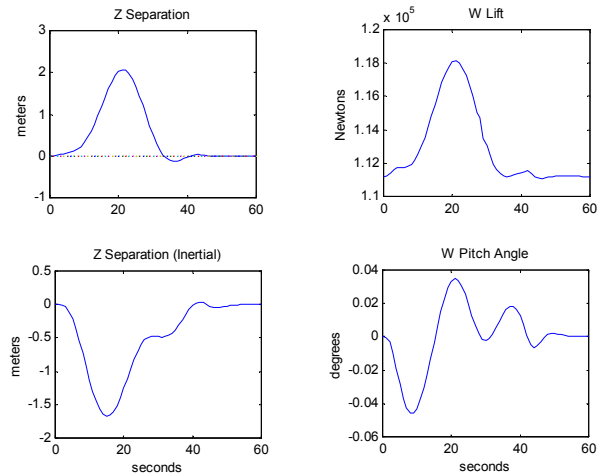


Figure 13. W's response to L heading change: route formation: z axis.

The most complex maneuver conducted in the simulation was the climbing turn. Fig. shows the three dimensional flight path of the formation as it climbed to a new altitude and turned left.

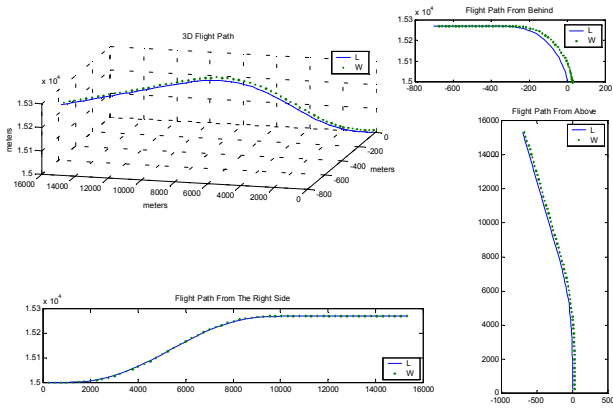


Figure 14. Flight path in climbing turn maneuver: inertial reference frame.

To move the formation to a new altitude and heading, the exogenous disturbance signals shown below were created by L. The amount of heading change and the distance climbed in this complex maneuver is less than in the individual maneuvers previously shown, because a more aggressive maneuver causes the automatic formation flight control system to become unstable.

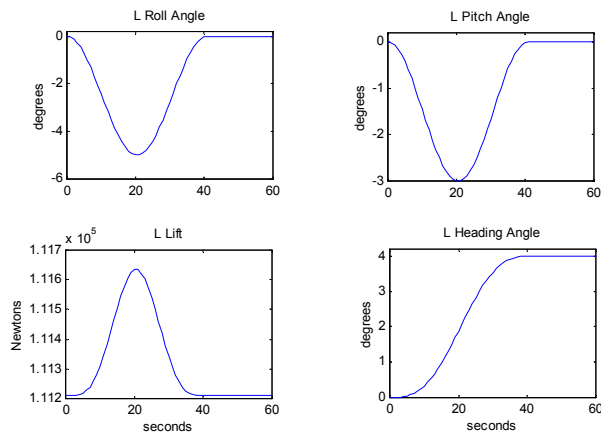


Figure 15. L simultaneous altitude and heading change maneuver.

The gains of both the first controller and second controller are listed in Table 2. The magnitude of the gains is meaningless until one considers the units associated with each control element; both control systems are low gain controllers.

Table 2. Automatic Formation Flight Control System Gains

| Symbol     | Controller 1 | Controller 2 | Units                   |
|------------|--------------|--------------|-------------------------|
| $K_{TP}$   | -1000        | -130         | N/m                     |
| $K_{TI}$   | -1000        | -130         | N/(m s)                 |
| $K_{TD}$   | 6000         | 2000         | N/(m/s)                 |
| $K_{TDD}$  | 0            | 5000         | N/(m/s <sup>2</sup> )   |
| $K_{LP}$   | -5000        | 1300         | N/m                     |
| $K_{LI}$   | -7000        | 1000         | N/(m s)                 |
| $K_{LD}$   | 12000        | -10000       | N/(m/s)                 |
| $K_{LDD}$  | 0            | -1000        | N/(m/s <sup>2</sup> )   |
| $K_{pP}$   | 0.008        | 0.0023       | rad/(m s)               |
| $K_{vceP}$ | -0.001       | 0            | rad/(m s)               |
| $K_{pI}$   | 0.008        | 0.0023       | rad/(m s <sup>2</sup> ) |
| $K_{pD}$   | -0.050       | -0.025       | rad/m                   |
| $K_{pDD}$  | -0.050       | -0.025       | rad/(m/s)               |

Finally, extensive simulation results are documented in Ref. [6].

## 6. CONCLUSIONS

The results of the nonlinear simulations validate the concept of three dimensional automatic formation flight control. However, the controller is sensitive to the amplitude of the disturbances, which is to say, aggressive L maneuvers can cause the automatic formation flight control system to become unstable. Controller robustness will become even more crucial when the aerodynamic coupling effects associated with flying tight formations are included in the simulation. Indeed the induced drag reduction afforded by close formation flight requires W to stay within +/- 5% of the stipulated optimal lateral separation during formation maneuvers, further limiting the amplitude of permissible L maneuvers. Hence, the maneuvers performed by L must be relatively benign for the controller to automatically maintain the formation.

## BIBLIOGRAPHY

- [1] Blake, William and Dieter Multhopp, "Design, Performance, and Modeling Considerations for Close Formation Flight," Proceedings of the 1999 AIAA Guidance, Navigation and Control Conference, Portland, OR, August 9-11, 1999, AIAA paper No 99-4343.
- [2] Pachter, M., J.Dargan, J. J. D'Azzo, "Automatic Formation Flight Control," AIAA Journal of Guidance, Control and Dynamics, Vol 17, No 6, Nov-Dec 1994, pp 1380-1383.
- [3] Pachter, Meir, Andrew W. Proud, and J. J. D'Azzo "Close Formation Flight Control," Proceedings of the 1999 AIAA Guidance, Navigation and Control Conference, Portland, OR, August 9-11, 1999, AIAA paper No 99-4112.

- [4] Proud, Andrew W., "Close Formation Flight Control," MS Thesis, AFIT/GE/ENG/99M-24, School of Engineering, Air Force Institute of Technology (AU), Wright-Patterson AFB, OH, March 1999.
- [5] Stevens, Brian L., Frank L. Lewis, Aircraft Control and Simulation, John Wiley & Sons, 1992.
- [6] Hall, James K., "Three Dimensional Formation Flight Control," MS Thesis, AFIT/GE/ENY/00M-06, School of Engineering, Air Force Institute of Technology (AU), Wright-Patterson AFB, OH, March 2000.